The Journal of Experimental Biology 200, 735–752 (1997)
Printed in Great Britain © The Company of Biologists Limited 1997
JEB0584

THE KINEMATICS OF SWALLOWING IN THE BUCCAL MASS OF *APLYSIA CALIFORNICA*

RICHARD F. DRUSHEL[1,*], DAVID M. NEUSTADTER[2,†], LORI LYN SHALLENBERGER[1,‡], PATRICK E. CRAGO[2] AND HILLEL J. CHIEL[1,3]

[1]*Department of Biology,* [2]*Department of Biomedical Engineering* and [3]*Department of Neurosciences, Case Western Reserve University, Cleveland, OH 44106, USA*

Accepted 25 November 1996

Summary

Changes in the positions, shapes and movements of the feeding apparatus (buccal mass) of the marine mollusc *Aplysia californica* were studied in intact, transilluminated juveniles. The buccal mass assumes characteristic shapes as its internal structure, the radula/odontophore, moves anteriorly (protracts) or posteriorly (retracts). These shapes are especially distinctive when the radula/odontophore has protracted forwards fully, is close to its resting or neutral position, or has retracted backwards fully. We refer to the shapes that occur at full protraction, transition and full retraction as shape 1 (spherical), shape 2 (ovoid) and shape 3 (Γ-shaped), respectively. We introduce this shape nomenclature in order to avoid confusion with the existing terms protraction and retraction, which we reserve exclusively to describe the direction of movement of the radula/odontophore.

The observed shape changes do not agree with those predicted on the basis of *in vitro* observations of a feeding head preparation, but are similar to shapes observed *in vitro* in the snail *Lymnaea stagnalis*. The buccal mass also rotates approximately 10° dorsally during retraction, pivoting on the attachment to the mouth, before the subsequent protraction and return of the buccal mass to the transition shape. This rotation may be due to activation of the extrinsic muscles of the buccal mass.

Plots of the buccal mass shape parameters eccentricity *versus* ellipticity create a two-dimensional shape space, which accurately quantifies the subtle transitions of shape between the different phases of the feeding cycle. Quantitative differences are observed between pure swallows and swallows with tearing behavior, but the qualitative shapes are similar. Hysteresis in the shape space plots of most swallows provides evidence for the hypothesis that protraction and retraction each have distinct 'active' and 'return' phases.

The observed kinematic pattern imposes constraints on the internal structures of the buccal mass and may be used to infer the shape and positions of the radula and odontophore.

Key words: kinematics, swallowing, slug, buccal mass, radula, shape space analysis, *Aplysia californica*.

Introduction

Adaptive behavior is likely to be the consequence of the interaction between a neural controller and the biomechanics of the body that it controls (Chiel and Beer, 1993). To demonstrate that this hypothesis is true, it is essential to study systems in which one can both analyze neural control in detail and characterize its interaction with the biomechanics of the periphery. Some progress has been made in relating the biomechanical properties of musculo-skeletal systems to the neural organization of the spinal cord in vertebrates (Bizzi *et al.* 1991). However, the complexity of the neural control of vertebrate systems has made it difficult to test this hypothesis directly. An alternative approach is to study simpler systems whose neural control and biomechanics are both tractable to detailed experimental analysis.

Molluscan feeding is a form of adaptive behavior that may be advantageous for studying the interaction of neural control and peripheral biomechanics. There have been extensive studies on the neural control of feeding in a wide variety of molluscs (Arshavsky *et al.* 1989*a*,*b*; Benjamin and Elliott, 1989; Bulloch and Ridgway, 1995; Croll *et al.* 1985; Delaney and Gelperin, 1990; Quinlan *et al.* 1995). These studies have clarified some of the mechanisms by which small neural networks can generate repetitive but flexible motor patterns.

The peripheral biomechanics of the feeding apparatus of

*e-mail: rfd@po.cwru.edu.
†Present address: MRI Division, Elscint Ltd, Advanced Technology Center, PO Box 550, Haifa 31004, Israel.
‡Present address: College of Medicine, Ohio State University, Meiling Hall, 370 West 9th Avenue, Columbus, OH 43210-1238, USA.

molluscs is also tractable to experimental analysis. The molluscan feeding apparatus – the buccal mass – is composed of muscle and cartilage (Starmühlner, 1956) with a relatively small internal vascular (hydrostatic skeletal) system (Drushel *et al.* 1993). Thus, these structures are examples of muscular hydrostats (Kier and Smith, 1985), structures, such as tentacles, tongues or trunks, that use muscle both for support and for generating force. Since higher vertebrates, including humans, use tongues as an integral part of their feeding apparatus, understanding the interaction between neural control and biomechanics in molluscs is likely to be of use for understanding feeding movements in more complex animals. Moreover, there has been recent interest on the part of roboticists in understanding the kinematics and dynamics of hyper-redundant structures, since these could serve as the basis for devices that could locomote over very irregular terrains or manipulate extremely irregular objects (Chirikjian and Burdick, 1995*a*,*b*). Thus, careful experimental studies of the control of biological muscular hydrostats might lead to new ideas for robotic design and control.

In order to investigate the interactions between neural control and biomechanics in adaptive behavior, we have chosen to study the marine mollusc *Aplysia californica*, whose feeding behavior has served as a model system for the study of complex adaptive behavior over the last two decades. Various forms of adaptive behavior have been characterized in *A. californica*: switching from swallowing to tearing as mechanical load increases (Hurwitz and Susswein, 1992), switching from swallowing to rejection in response to inedible food (Kupfermann, 1974; Morton and Chiel, 1993*a*,*b*), arousing and satiating in response to food stimuli (Kupfermann, 1974; Weiss *et al.* 1982), choosing among feeding or other behaviors (Ziv *et al.* 1991), and learning that food is inedible (Chiel and Susswein, 1993; Susswein *et al.* 1986).

Considerable progress has been made in clarifying the neural basis of some of these adaptive behaviors. For example, Teyke *et al.* (1990) characterized a single neuron, the cerebral-pedal regulator, that suppressed withdrawal responses, increased blood pressure and provided excitation to neurons that trigger and maintain feeding responses, suggesting that this neuron could play a role in behavioral choice by activating feeding behavior and suppressing other behavioral states.

However, recent work has suggested the importance of understanding the biomechanics of the feeding apparatus of *A. californica*, the buccal mass, in order to understand properly the control and execution of other adaptive behaviors. For example, Morton and Chiel (1993*a*,*b*) showed that the biomechanical correlate of switching from ingestion to rejection was a change in the timing of radular closure relative to the protraction/retraction cycle of feeding. More recently, Hurwitz *et al.* (1994, 1996) have shown that the neurons initiating the protraction phase of feeding motor programs, B31/B32, are also motor neurons for a buccal mass muscle, I2, that mediates protraction. Furthermore, extensive work over the last two decades has demonstrated that the musculature of the buccal mass is subject to neuromodulation (for a review, see Katz and Frost, 1996), and functional consequences of this modulation have been predicted (Weiss *et al.* 1992), but the behavioral effect of modulators has not been studied in the intact buccal mass. These results suggest that a better understanding of the mechanisms of the adaptive behavior of *A. californica* will require a more complete understanding of the kinematics and kinetics of its buccal mass.

Prior work in *Aplysia* has suggested specific hypotheses about the kinematics of the buccal mass and the functions of its constituent muscles. Functional anatomical studies of the dissected buccal mass of *Aplysia punctata* by Howells (1942) and of *Aplysia californica* by Scott *et al.* (1991) suggested specific roles for different muscles of the buccal mass. Based upon studies of a semi-intact preparation, Weiss *et al.* (1986) proposed a sequence of radula/odontophore movements during the bite–swallow cycle in *Aplysia californica*, with accompanying diagrammatic predictions of radula/odontophore position and buccal mass shape. These indicate a rigid radula/odontophore which rotates through 180 ° (peak protraction to peak retraction), with little effect on buccal mass shape except during protraction, at which point the shape resembles a small ball instead of a broad oval. Weiss *et al.* (1986) also distinguish symmetrical ‘active’ and ‘return’ phases of both protraction and retraction movements (i.e. the movement of the radula/odontophore from peak protraction to the resting state is the mirror image of the movement from rest to peak protraction). The timing of the forward/backward movements is observed to be variable, however, and the ‘active’ and ‘return’ phases are hypothesized to be under the control of separate oscillators.

Work in related species has also suggested hypotheses about the kinematics of molluscan buccal masses. However, the buccal mass movements and shape changes which have been observed in other molluscs may not be reasonable predictors of those in *Aplysia*. For example, the isolated buccal mass of the snail *Lymnaea stagnalis* undergoes distinctive shape changes during spontaneous feeding cycles *in vitro* (Rose and Benjamin, 1979); these authors mention, but do not illustrate, that similar changes were also observed in intact, semi-transparent, laboratory-reared animals. While the buccal mass musculature of *Lymnaea stagnalis* appears similar to that of *Aplysia*, the internal structure of the odontophore is different: the odontophoral ‘cartilages’ or bolsters of *Aplysia* are not as discrete and well-organized (Eales, 1921; Starmühlner, 1956; Drushel *et al.* 1993). In addition, *Lymnaea* feeds by rasping movements of both the odontophore and the radula (independent of the odontophore) against the substratum (Carriker, 1946), while *Aplysia* actively grabs food by protracting the radula with its halves open, closing it upon the food and then retracting the closed radula (Howells, 1942; Kupfermann, 1974). These important differences in anatomy and feeding mechanism make it unwise to argue by simple analogy that *Aplysia* must be similar to *Lymnaea*.

A reference standard of buccal mass movements in intact, unoperated *Aplysia* is needed to supplement observations made solely on the basis of anatomy or from *in vitro* preparations.

In vivo kinematics provides a method to evaluate the degree to which a particular *in vitro* preparation still functions as *in vivo*. A major uncertainty in the use of dissected and *in vitro* preparations is the possible presence of artifacts due merely to surgery or dissection. The existence of a reference kinematic standard would allow such artifacts to be detected as deviations from that standard. This could also lead to improved experimental techniques which minimize such artifacts, making possible more accurate analyses.

In the present study, we created a reference standard for the kinematics of the *Aplysia californica* buccal mass during swallowing *in vivo* using transilluminated juveniles to observe directly the buccal mass non-invasively *in situ*. We find that the *A. californica* buccal mass has different shapes at the peak of radular protraction, at the peak of radular retraction and at the transition between these extremes. The shapes agree qualitatively with those observed in *Lymnaea stagnalis* (Rose and Benjamin, 1979), but not with those predicted for *A. californica* by Weiss *et al.* (1986). We describe rotational movements of the buccal mass proper which are correlated with, but do not appear to be caused by, specific shape changes and may reflect the activity in the extrinsic musculature. In addition, by making precise quantitative measurements of shape change, we are able to demonstrate a kinematic basis for the 'active' and 'return' phases of protraction and retraction *in vivo;* however, these phases are generally not symmetrical. Finally, by using the kinematics as physical constraints, we offer improved predictions of the internal position and shape of the radula/odontophore during the feeding cycle.

Portions of this work have appeared in preliminary form (Neustadter *et al.* 1992; Drushel *et al.* 1994). The use of transilluminated juveniles was suggested by I. Kupfermann (personal communication).

Materials and methods

Transillumination studies

Preparation of animals

Juvenile specimens of *Aplysia californica* (Cooper) (10–20 mm long) were obtained from the *Aplysia* Resource Facility at the University of Miami (Miami, Florida, USA), maintained in small breeder nets suspended in a tank of aerated artificial sea water (Instant Ocean; from Aquarium Systems, Mentor, Ohio, USA) at 15–20 °C and fed daily on seaweed (*Gracilaria* sp.; from Marinus, Inc., Long Beach, California, USA, stored frozen until fed to the animals). Prior to use in feeding studies, slugs were starved for 1–2 days, and only animals showing vigorous responses to seaweed were selected as subjects. Because slugs of this size have little skin pigmentation, they are relatively transparent; when transilluminated, the shadow outline of the buccal mass is clearly and sharply visible inside the head. The basic strategy was to induce transilluminated slugs to feed upon thin-cut strips of seaweed, and then to record the feeding behavior with a video camera attached to a dissecting microscope.

One-axis views

Preliminary observations of feeding in over 20 different transilluminated slugs were made in lateral view, with a single fiber-optic light source and dissecting microscope/video camera. While adequate to observe qualitative changes in buccal mass shape during feeding, this one-axis arangement did not allow rigorous control of parallax: it was difficult to determine whether the slug's head was truly perpendicular to the image axis. Since the shape of the buccal mass shadow changes with illumination/viewing angle, measurements made from such shadows would be inaccurate if perpendicularity were not maintained. Moreover, the geometry of the one-axis arrangement made it difficult to feed the slugs: the image axis was vertical, requiring the slugs to lie upon their sides while eating, a position they did not seem to favor.

A complete quantitative shape space analysis (see below) was performed upon swallowing sequences recorded using the one-axis arrangement (data not shown). The sequences selected were judged to be relatively free of parallax, although this could not be verified directly. The quantitative results are in close agreement with those ultimately obtained using a more precise two-axis arrangement (see below).

Two-axis views

On the basis of these preliminary experiments, a two-axis apparatus was constructed to control parallax and to allow the slugs to assume a more natural feeding posture (Fig. 1A). Two dissecting microscopes with video cameras were positioned at right angles, one vertical and one horizontal. A jig held two fiber-optic lights at right angles, and the image axes of the microscopes were aligned with the lights. Light levels were controlled with fixed-aperture diaphragms. A water chamber for slugs was built from glass microscope slides and attached by a steel support arm to a three-axis micromanipulator. Slugs were elevated off the bottom of the glass box by a small glass shelf; this prevented them from being obscured in lateral view by the silicone rubber used to seal the joints of the glass walls with the base. The glass box was positioned using the micromanipulator such that the intersection of the horizontal and vertical image axes would fall inside the head of a slug placed foot-down upon the glass shelf. The box was large enough in all dimensions such that the water meniscus at the edges (a possible source of image distortion) was well outside both fields of view.

A state of food arousal was induced in slugs by touching pieces of seaweed held in forceps to their rhinophores and anterior tentacles, and observing that they made several biting responses as they attempted to consume the seaweed. A slug was then placed onto the glass shelf inside the chamber, which was filled with aerated artificial sea water at 15–20 °C. To minimize bubbles and vibration, the water in the box was neither actively aerated nor cooled; it was changed approximately every 10 min from an aerated, cooled external stock by syringe. Thin strips of *Gracilaria* (less than 0.5 mm wide, cut with a razor blade) were presented to the lips of the slug with fine forceps. When the food had been seized by the radula (after a bite), the slug was quickly oriented to be

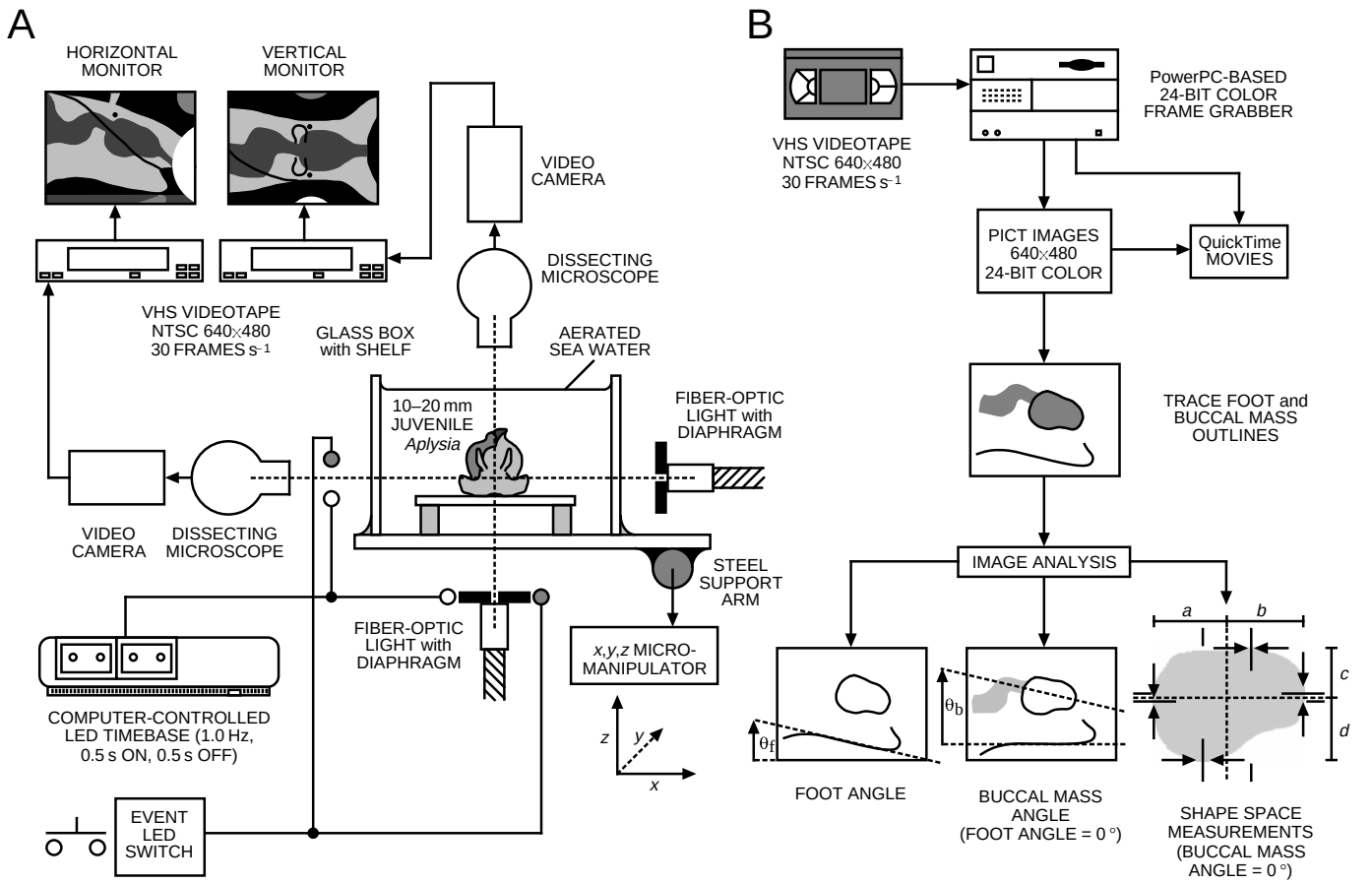

Fig. 1. Summary of transilluminated slug image recording and analysis. For details, see Materials and methods. (A) Two-axis, right-angled video camera arrangement, showing placement of glass feeding chamber, transillumination lamps and camera synchronization LED indicators. (B) Frame-grabbing and video image analysis flow diagram.

perpendicular to the lateral-view microscope/camera, using forceps to move the entire animal, and the *x,y* controls of the micromanipulator to move the glass box. Live television displays of both horizontal and vertical views were used to verify correct orientation, and minor corrections were made with the micromanipulator as necessary. Data from each view were recorded simultaneously to color NTSC video tapes (30 frames s^{-1}).

Camera synchronization

Event marker light-emitting diodes (LEDs) were positioned in each field of view, all illuminated by a single momentary pushbutton switch. To provide a synchronized timebase at high resolution, however, an interface card was constructed for a Coleco ADAM microcomputer, which flashed two additional timebase LEDs at 1.0 Hz (on 0.5 s, off 0.5 s) under software control (Fig. 1A). This flashing frequency corresponds to 15 frames of NTSC video for each on and off state. Tests showed that a one-frame loss of synchrony between video tapes from the two camera views occurred at approximately 5 min intervals. Since typical slug feeding sequences were only 30 s long, this method of synchronizing the two views was considered adequate.

Image analysis

Data selection

Transilluminated *A. californica* were video-taped using both the one-axis and two-axis microscope/camera arrangements. More than 20 animals were observed using the single-axis microscope/camera arrangement in 89 different sequences for a total time of more than 25 h, during which 1960 swallows and tears were observed and approximately 15 bites. Five animals were observed using the two-axis microscope/camera arrangement in 37 different sequences for a total time of more than 5.5 h, during which 308 swallows and tears were observed and five bites. From this extensive collection of recorded feeding behavior, a single feeding sequence of nine consecutive swallows (32 s total) was selected for detailed quantitative analysis. This sequence was recorded using the two-axis apparatus and had the most precise control of slug alignment and parallax along both axes. On the basis of careful analysis of the entire video record, we believe that this sequence is representative of all the swallowing movements observed in transilluminated slugs.

The selected feeding sequence consists of two distinct behavioral periods: an initial train of pure swallows (swallows

1–4), and a final train of swallows with some tearing behavior (swallows 5–9). During the first four swallows, the seaweed moved in smoothly a distance of 0.39 mm, 0.55 mm, 0.71 mm and 0.78 mm, respectively, for a total distance of 2.43 mm, at which point it was no longer visible outside the animal. (The total length of the seaweed is unknown, but it was somewhat longer than 2.43 mm; several unrecorded bites and swallows occurred before the first swallow that we analyzed.) At the fourth retraction, the seaweed had reached the posterior buccal cavity and was lodged against the opening into the esophagus (note that the minimum length from the jaws to the esophagus indicated in Fig. 3I is 3.89 mm). During each subsequent retraction, a discrete piece of seaweed was clearly observed to move down the translucent esophagus. A reasonable inference is that the animal had succeeded in tearing off a piece of seaweed, since the seaweed was strong enough that it was unlikely to break simply by being pulled inwards. Further support for this hypothesis was the observation that some of these retractions were so vigorous that, when a chunk of seaweed was torn off, the radula/odontophore snapped posteriorly and its anterior tip caused the dorsal roof of the buccal cavity to bulge outwards (swallows 7, 8 and 9). These results are consistent with the observations of Hurwitz and Susswein (1992) in adult *A. oculifera*, which is the basis for our use of the term 'tearing' to describe this behavior. In these same juvenile *A. californica*, we observed similar movements as they fed freely on larger pieces of *Gracilaria*. The animals thrived on this diet and grew steadily, suggesting that this food was not too tough for them to consume. Moreover, by cutting the seaweed into longitudinal strips, we reduced the forces necessary to consume it, and thus it was unlikely to have distorted the ingestive movements made by the animals. The quantitative differences between the pure swallows and the swallows/tears are detailed in the Results section.

It was difficult to observe biting behavior while maintaining the precise alignment of the slugs relative to one or two viewing axes, because the heads of the animals are much freer to move during biting, whereas during swallowing the strip of seaweed provides a natural axis of orientation. Typically, bites and several swallows had occurred by the time proper alignment was established. Bites observed by direct illumination did not appear to differ from bites observed in adult slugs (i.e. the jaws opened wide, the radula protracted open through the jaws, then retracted while closing). The discussion of full protraction in Fig. 10D (below) is based on careful examination of QuickTime digital movies (see below) made from the few observations of biting that we were able to obtain. Because these recordings were not properly aligned, we did not analyze them further.

Digitizing of images

Video frames from the lateral-view and dorsal-view video tapes were displayed one at a time ($30\,s^{-1}$) and digitized with a RasterOps 24STV frame grabber in an Apple Power Macintosh 7100/66AV computer (Fig. 1B, top). Each PICT-format image was 640×480 pixels, 24-bit RGB color. Flashes of the event LEDs and timebase LEDs were used to synchronize the images. Digital movies in QuickTime format were also utilized in order to simplify study of movements at the single-frame level, forwards and backwards, beginning at known frames. QuickTime movies were created both in real time, by playing the video tape through the frame grabber, and by pasting individual frames sequentially into a movie. This kind of precision analysis is impossible using a standard VCR with still/frame-advance features.

Angular analysis

Two angular parameters were defined: *foot angle* (between the anterior foot and the substratum) and *buccal mass angle* (between the long axis of the buccal mass and the anterior foot). Both angles were measured from PICT images of alternate video frames using Canvas 3.5.3 graphics software (Deneba Software) to draw axis lines directly on the images (and to provide the slope, dy/dx, for manual calculation of angles in degrees). For the foot angle, a line was drawn through the flattest region of the anterior foot (Fig. 1B, bottom left). For the buccal mass angle, the image was first rotated such that the foot angle was zero, and a line was then drawn from the midpoint of the jaw region of the buccal mass to the exit of the esophagus (Fig. 1B, bottom center). While the anterior esophagus often exited the buccal cavity in a straight line, this line was not necessarily aligned with the buccal mass axis; consequently, the exit point only was used as a landmark. All angles are accurate to ±1 °.

Quantitative shape parameters

Characteristic qualitative changes in buccal mass shape were observed in lateral view during feeding in transilluminated slugs (see Results). To characterize the many intermediate shapes better, however, a quantitative shape analysis was developed. The buccal mass shape can be approximated by four ellipse quadrants (Fig. 2A). Given antero-posterior axis lengths a and b (b is most anterior) and dorso-ventral axis lengths c and d (c is most dorsal), we define two shape parameters:

$$\text{ellipticity} = \left(\frac{c+d}{a+b} \right) - 1 , \qquad (1)$$

and

$$\text{eccentricity} = \left(\frac{b}{a+b} \right) - 0.5 . \qquad (2)$$

Ellipticity quantifies the degree to which a shape is like an ellipse. An ellipse wider than it is tall has negative ellipticity, whereas an ellipse taller than it is wide has positive ellipticity. A circle, being as wide as it is tall, has zero ellipticity. *Eccentricity* quantifies how skewed a shape is to one side or the other. A shape with $b>a$ (center skewed to the left) has positive eccentricity, whereas a shape with $a>b$ (center skewed to the right) has negative eccentricity. A circle has zero eccentricity.

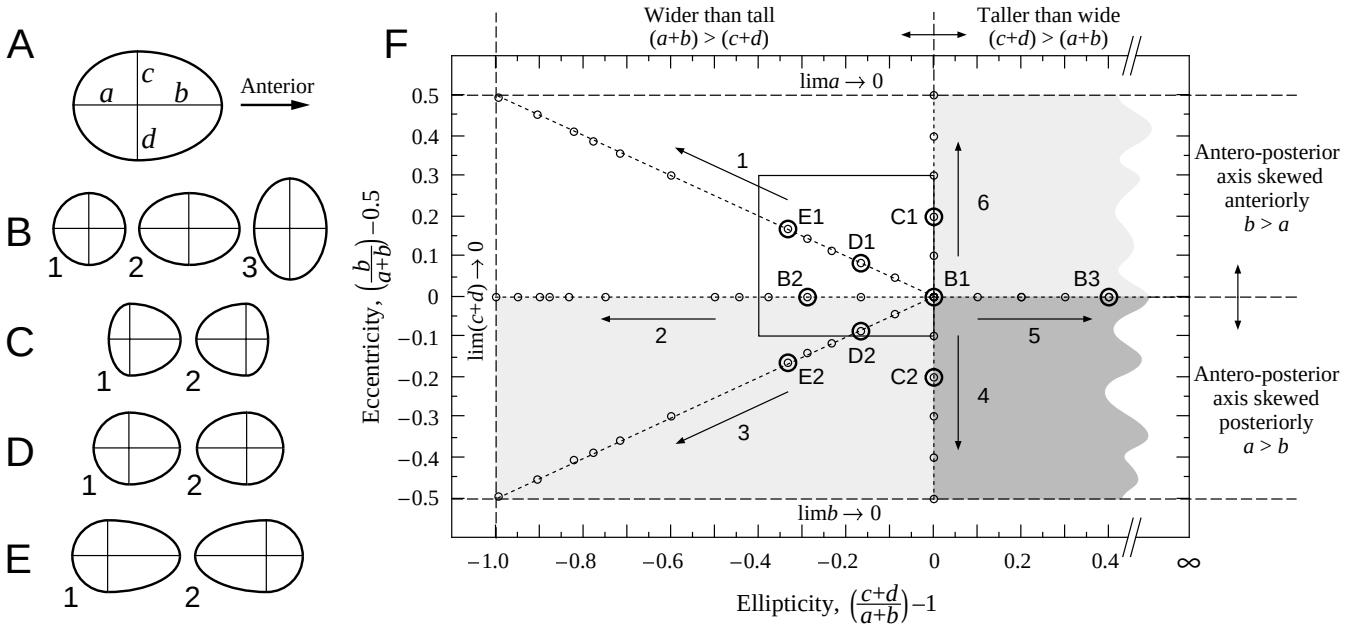

Fig. 2. Rationale for the analysis of buccal mass shapes using an artificial shape space. (A) The buccal mass can be approximated by four ellipse quadrants, giving four measurable distances *a*, *b*, *c* and *d*. The shape parameters ellipticity and eccentricity are calculated from these measurements (see Materials and methods). (B–E) Sample shapes. Points in shape space corresponding to each shape are shown in F. (F) Shape space plot of eccentricity *versus* ellipticity. Shape space is bounded on three sides and extends to infinity on the fourth. The small box shows the approximate range of shape space values observed *in vivo*. Six different lines of parameter variants are shown to illustrate the non-linearity of shape space. For lines 1–3, the parameter that is varied changes through the values 50, 60, 70, 80, 90, 100, 200, 300, 400, 500, 1000 and 10 000; the other parameters are held constant at 50. Line 1: *b* varies. Line 2: *a* and *b* vary equally. Line 3: *a* varies. For lines 4 and 6, both *a* and *b* are varied, but the sum $a+b=100$. The first parameter that is varied changes through the values 50, 60, 70, 80, 90 and 100, the second changes to keep the sum constant, and $c=d=50$. Line 4: *a* varies first. Line 6: *b* varies first. For line 5, the sum $c+d$ is changed through the values 100, 150, 200, 250 and 300, and the sum $a+b=100$.

Shape space analysis

A plot of eccentricity *versus* ellipticity forms a two-dimensional region which we term *shape space* (Fig. 2F). Complex changes in shape translate into movements through different regions of shape space. While the overall shape space is not linear (it is bounded on three sides and extends to infinity on the fourth), shapes observed in transilluminated feeding slugs *in vivo* fall into a small region of little spatial distortion (Fig. 2F, box; see Results).

Buccal mass measurements

PICT images of alternate frames were displayed on a color monitor, and the outlines of the foot and the buccal mass were traced onto clear acetate sheets. Ambiguities in the buccal mass outline were resolved by study of the appropriate QuickTime movie sequence around the frame in question. In general, the dorsal and ventral outlines were quite unambiguous. A best-estimate smooth curve was drawn through the posterior esophageal region to connect the dorsal and ventral outlines. The anterior shadow of the seaweed strip was subtracted out by estimating the location of the mouth opening (based on the dorsal camera view). The tracings were digitized using a flatbed scanner, and TIFF-format images of each buccal mass outline were extracted manually using Canvas 3.5.3 graphics software. The final images were solid black shapes on a white background.

The measurement of the *a*, *b*, *c* and *d* parameters from TIFF images was automated using custom-designed software written in QuickBASIC 4.5 (Microsoft) on an 80486DX2-66 computer. Shapes were first rotated such that the buccal mass angles were 0°, using the foot and buccal mass angles measured previously. Aliasing artifacts from rotating the bitmaps were smoothed out by the software. The following algorithm was used to determine the parameters from rotated, smoothed images (Fig. 1B, bottom right). The bounding rectangle was found for each shape, giving the quantities $a+b$ and $c+d$. The division between *a* and *b* was set midway between the points of maximum convexity on the top and bottom. Similarly, the division between *c* and *d* was located midway between the points of maximum convexity on the left and right. This method gave good results even when shapes had slight concavities on one surface, giving two convexities instead of one.

Video jitter, tracing inaccuracies and aliasing effects from image scanning all lead to a small amount of high-frequency noise in the final TIFF images of the buccal mass outlines. This noise clearly does not represent the movements of the animal, whose fastest movements occur over the course of 1 s.

Measurements were therefore smoothed by the method of running average (five points for each average, centered about each data point in turn; the duration of the five points was equivalent to 1/3 s). Smoothing the measured *a*, *b*, *c* and *d* values and then calculating ellipticity and eccentricity was not observably different from calculating the latter from the raw *a*, *b*, *c* and *d* values and then smoothing the results (data not shown).

Nomenclature: protraction and retraction

To avoid ambiguity, in all subsequent discussion, we reserve the terms *protraction* and *retraction* exclusively for reference to the movements (observed or presumed) of the radula/odontophore. Specifically, protraction is defined as *any* forward (postero-anterior) movement of the radula/odontophore and retraction is defined as *any* backward (antero-posterior) movement of the radula/odontophore. In earlier literature, these terms have been ambiguously applied to both the radula/odontophore and the buccal mass. In the present paper, we do not use the terms protraction and retraction to refer to movements of the buccal mass.

Results

Qualitative and quantitative shape changes

The *Aplysia californica* buccal mass undergoes characteristic shape changes during swallowing *in vivo*, as seen in lateral and dorsal views of transilluminated juveniles. At full retraction, the buccal mass is very asymmetric in lateral view, assuming a Γ-shape which is constricted anteriorly (Fig. 3A,G). A ventral projection, corresponding to the radular stalk, extends posteriorly past a reference transverse plane through the eyespot (Fig. 3G). At full protraction, however, the buccal mass appears rounded in both lateral (Fig. 3C,I) and dorsal (Fig. 3F,L) views; it is roughly spherical and has reached its minimum antero-posterior length and maximum medio-lateral width. At full protraction, the buccal mass is almost completely anterior to the reference eyespot plane (Fig. 3I), and the point of maximum medio-lateral width is at its most anterior extent (Fig. 3L). Viewed dorsally, at full retraction, the buccal mass is elliptical, elongated along the antero-posterior axis but narrower than in full protraction (Fig. 3D,J). Between full protraction and full retraction, the buccal mass assumes a stable intermediate shape. The buccal mass appears ovoid in lateral view, lacking the dominant anterior constriction seen in full retraction (Fig. 3B,H); in dorsal view, the buccal mass is elliptical (Fig. 3E,K). We hereafter refer to these distinct shape classes (spherical, ovoid and Γ-shaped) as shapes 1, 2 and 3, respectively. Note that Weiss *et al.* (1986) use the term ‘rest’ to describe the buccal mass state intermediate between peak protraction and peak retraction, regardless of how it is reached. We prefer the term ‘transition’ to avoid the implication that these states are identical to those assumed by the buccal mass when the slug is truly at rest, i.e. not actively feeding.

Timing

The timing of different phases of the feeding cycle can be determined by measuring the intervals between several unambiguous buccal mass movements, which are used as landmark events. The peaks of protraction and retraction are obvious as the points of maximal anterior and posterior extent, respectively, of the buccal mass. At a point shortly after peak retraction, the buccal mass suddenly loses its anterior concavity and changes from Γ-shaped to oval-shaped (shape 3 to shape 2). Another clearly discernible landmark is the sudden anterior movement of the buccal mass after a period of quiescence in the transition phase that occurs after the peak of retraction; we refer to this as the onset of the second half of protraction (i.e. the movement of the radula from transition to full protraction).

Using these landmark events, we define the following time intervals: *t1* [peak protraction (shape 1) to peak retraction (shape 3)], *t2* (peak retraction to the loss of shape 3), *t3* (loss of shape 3 to the start of forward buccal mass movement in the second half of protraction) and *t4* [(second half of protraction to peak protraction (shape 1)]. Note that the times of appearance of the shape classes 1, 2 and 3 do not necessarily correspond to the *t1*–*t4* intervals. Shape 1 (the spherical shape) is present during the end of *t4* and the start of *t1*; shape 3 (Γ-shape) is present during the end of *t1* and all of *t2*. Shape 2 (ovoid), which occurs during protraction, exactly occupies *t3* by definition; but there are no such boundaries for the transition shape seen during the progress from protraction to retraction (which occurs during *t1*). This lack of correspondence is because there are no unambiguous criteria available to distinguish intermediate buccal mass shapes on the basis of shape class alone (see Fig. 3 legend, relating shapes to time intervals).

Timing for the intervals *t1*–*t4* for each of nine consecutive swallows is presented in Table 1. In the swallows studied, the mean feeding cycle (peak protraction to peak protraction) lasted 3.45±0.15 s (mean ± S.E.M.). The retraction phase (peak protraction to peak retraction, *t1*) occupied 40 % of the feeding cycle. Shape 3 (Γ-shape) persisted for a short while after peak retraction (*t2*, 11 %). Shape 2 (ovoid) was found throughout the *t3* interval (25 %). The remainder of the feeding cycle (start of forward buccal mass movement in the second half of protraction to peak protraction, *t4*, 24 %) was occupied by the transition from shape 2 to shape 1.

The *t3* interval is a period of *stable transition*: the buccal mass shape is relatively constant for the entire interval, unlike the *dynamic transition* occurring during retraction. It is clear from repeated examination of the video records that the change in the shape of the buccal mass from peak protraction to peak retraction is continuous, whereas after the peak of retraction, the buccal mass assumes shape 2 and remains in that shape for some brief interval before the onset of the second half of protraction.

For swallows 1–4, the average values of the intervals *t1*–*t4* and the average cycle lengths are not statistically different from the average values for swallows 5–9, even though these

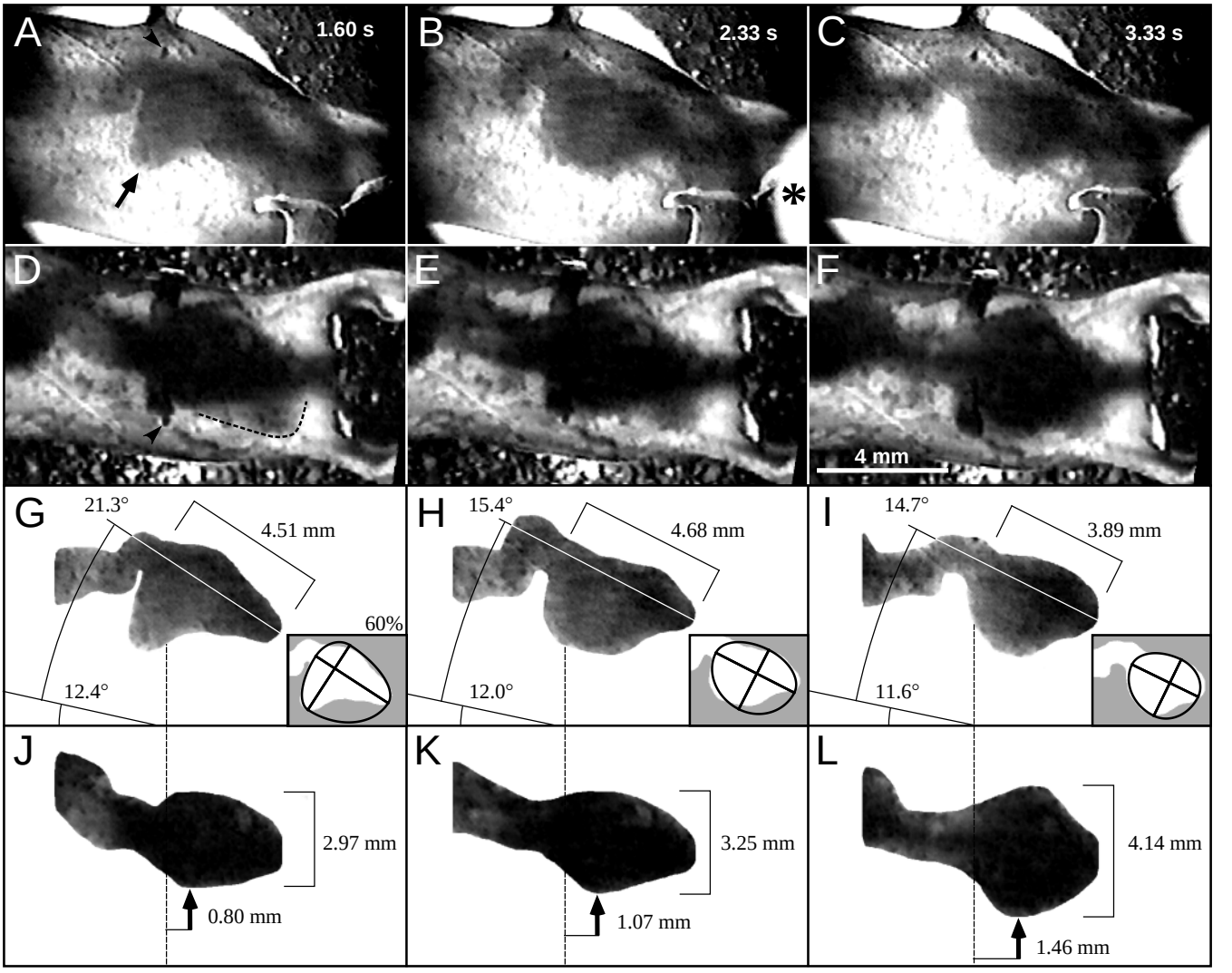

Fig. 3. Perpendicular lateral and dorsal views of transilluminated juvenile *Aplysia californica* during swallowing *in vivo*, showing buccal mass shapes at full retraction, transition and full protraction. This representative sequence is the fourth of nine consecutive swallows. (A) Full retraction, lateral view, 1.60 s after prior full protraction (0.00 s), at the *t1*/*t2* boundary. The buccal mass has a Γ-shape and the radular stalk protrudes ventrally (arrow). Note that the rhinophores are aligned, indicating minimal parallax in lateral view. The arrowhead marks the eyespot. (B) Stable transition between full retraction and full protraction, lateral view, 2.33 s after prior full protraction, at midpoint of *t3* interval. The buccal mass has an oval shape, and the antero-ventral concavity seen in retraction has become convex. The asterisk marks the flash of the 1.0 Hz timebase LED. (C) Full protraction, lateral view, 3.33 s after the previous full protraction, at the *t4*/*t1* boundary. The buccal mass is rounded. *t1*–*t4* are defined in Results. (D,E,F) Dorsal views corresponding to A, B and C above. The buccal mass shape changes from oval at full retraction to rounded in full protraction. The penis casts a faint shadow (dotted line, D) which must be subtracted to give the true buccal mass shape. The arrowhead marks the eyespot. Note that the rhinophores are centered on the head, indicating minimal parallax in dorsal view. (G–L) Isolated buccal mass shapes from A–F above, showing outlines as determined from color originals and repeated study of the movie sequence. For additional details, see Materials and methods. The vertical dashed lines are a reference transverse plane through the eyespot. Buccal mass dimensions (antero-posterior length, medio-lateral width and the point of maximum medio-lateral width relative to the eyespot plane) and angular changes shown in G–L are detailed in Results. Insets in G, H and I show ellipse quadrants derived from shape space measurements (see Figs 2A, 8D) superimposed upon the *in vivo* tracings. In G and I note that, while the buccal mass shapes are clearly different, the antero-posterior length of each is almost the same as the corresponding dorso-ventral length, leading to similar values of the ellipticity shape space parameter (see Fig. 6, swallow 4). The implications of such non-uniqueness of individual shape space parameters is considered in the Discussion. Note: the grayscale images shown here were converted from 24-bit color originals and contrast-enhanced using Adobe Photoshop 2.5.1 software (Adobe Systems). All actual measurements and analysis were performed on the color originals. The isolated buccal mass shapes shown in G–L and the eyespot plane were created for illustrative purposes only and were not used in the main data analysis.

swallows involve tearing (Table 1). Swallow 8 and especially swallow 9, however, have time intervals and total lengths that are least similar to the mean values, having the longest and shortest feeding cycle times, respectively.

Table 1. *Feeding cycle timing for* Aplysia californica *in nine consecutive swallows*

Swallow in sequence	Peak protraction to peak retraction, *t1* (s)	Peak retraction to loss of shape 3, *t2* (s)	Loss of shape 3 to forward buccal mass movement, *t3* (s)	Forward buccal mass movement to peak protraction, *t4* (s)	Total (s)
1	1.40	0.40	0.47	0.80	3.07
2	1.27	0.40	0.80	0.87	3.34
3	1.60	0.40	0.80	0.80	3.60
4	1.60	0.40	0.80	0.53	3.33
5	1.33	0.40	0.73	0.87	3.33
6	1.20	0.33	1.33	0.93	3.79
7	1.27	0.33	1.20	0.87	3.67
8	1.60	0.47	1.40	0.80	4.27
9	1.27	0.27	0.33	0.80	2.67
Mean 1–4*	1.47	0.40	0.72	0.75	3.34
S.E.M.	0.08	0.00	0.08	0.07	0.11
Mean 5–9†	1.33	0.36	1.00	0.85	3.55
S.E.M.	0.07	0.03	0.20	0.03	0.27
Mean 1–9	1.39	0.38	0.87	0.81	3.45
S.E.M.	0.06	0.02	0.12	0.40	0.15

*Swallows 1–4 are pure swallows with no head movement.
†Swallows 5–9 include some tearing behavior and increased ventral flexion of the head.
Mean times for swallows 1–4 do not differ significantly from those for swallows 5–9 (paired *t*-test; *P*-values range from 0.19 to 0.52).

Angular changes

The entire buccal mass undergoes rotational movements in addition to changing shape. Repeated viewings of the sequence of nine consecutive swallows, both of the original video tape and of digitized QuickTime movies (in which there was more precise frame-by-frame forward/backward control), revealed that the entire buccal mass appeared to move dorsally during radular retraction, then return to a more ventral position during stable transition and the movement from shape 2 to shape 1. Specifically, the buccal mass seemed to pivot dorsally and ventrally about a fixed point corresponding to the anteriormost end of the buccal mass, where the seaweed was entering the jaws. To verify this qualitative observation, the angular changes in the long axis of the buccal mass were measured, after subtracting out the angular changes in the anterior foot relative to the floor of the glass observation chamber (Figs 1B, 3G,H,I; also see Materials and methods).

In the studied sequence of nine consecutive swallows, the anterior foot angle increased with no obvious pattern from 6° to 22° (Fig. 4, solid line). After subtracting out the anterior foot angle, however, the buccal mass shows a periodic change in angle for swallows 1–7 (Fig. 4, circles). Buccal mass angle is maximal at peak retraction (range 22–36°) and minimal at peak protraction (range 12–25°); for any given swallow, the angular difference is approximately 10°. Most of the swallows also exhibit minor peaks of buccal mass angle in mid-*t4* (during the movement from shape 2 to shape 1). The buccal mass angle changes appear to lose periodicity during swallows 8 and 9, the end of this particular feeding sequence.

Note that a wandering baseline remains in the buccal mass angle changes, which does not appear to correlate with the foot angle changes. The baseline minimum at the swallow 4/5 boundary, however, is during the transition from pure swallows to swallows with some tearing behavior.

Normalized buccal mass angle changes

The overall regularity of buccal mass angle change suggests that all nine swallows share common kinematics of buccal mass angular movement. However, the presence of the wandering baseline in the buccal mass angle *versus* time plot makes it difficult to determine the rates of change during different phases of the feeding cycle. Consequently, the data for buccal mass angle were normalized. Baseline variability was removed by shifting all the peaks of protraction to a common baseline, then rescaling each swallow such that the peak protraction angle of each swallow was 100 % and rescaling the timebase such that the intervals *t1–t4* were equal to the mean *t1–t4* lengths (Fig. 5). A typical pure swallow, such as swallow 1 (Fig. 5A), shows a sharp increase in buccal mass angle during mid-*t1* (retraction), after a brief period of slower rise. The buccal mass angle falls sharply after peak retraction (*t1*/*t2* boundary), then falls more slowly during *t3* (stable transition) until the start of the second half of protraction (*t3*/*t4* boundary), during which it briefly rises and then falls to its minimum at the next peak of protraction (*t4*/*t1* boundary). When all nine swallows are averaged (Fig. 5B), the same behavior is observed, except that the ‘shoulder’ of slower decrease during *t3* is absent. This could be a consequence of combining pure swallows with swallows containing tearing behavior.

Shape space analysis

Time plots of the shape parameters ellipticity and

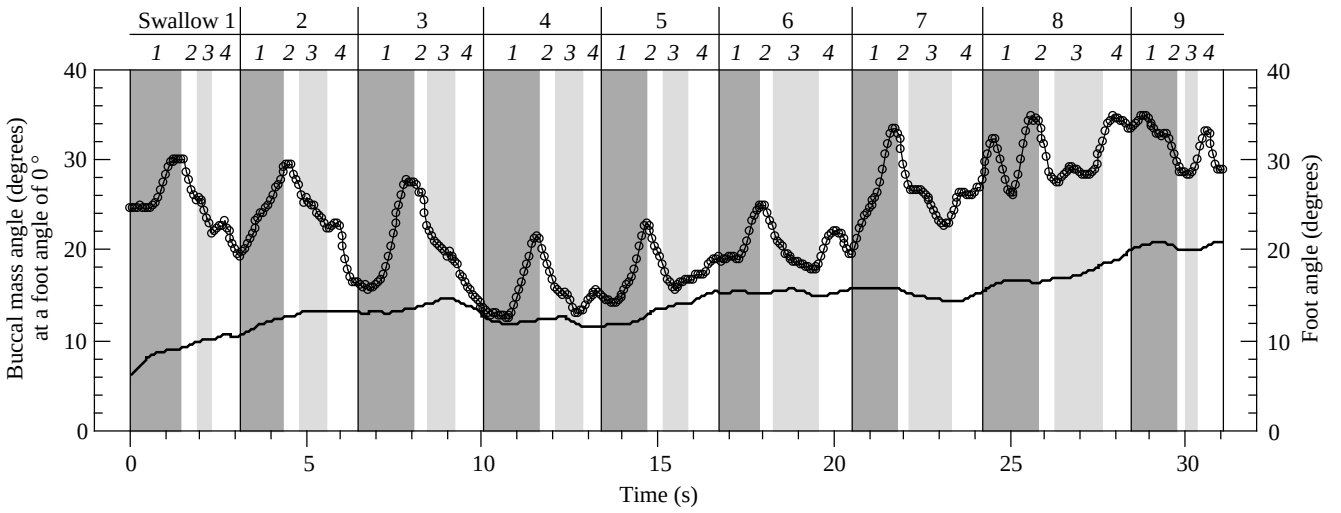

Fig. 4. Plot of foot angle (solid line, bottom) and buccal mass angle (at a foot angle of 0°, i.e. after subtracting out the anterior foot angle) (circles, top) *versus* time for nine consecutive swallows. Each swallow is delimited by a vertical line, and the *t1–t4* intervals (peak protraction to peak retraction, peak retraction to the loss of shape 3, loss of shape 3 to the start of forward buccal mass movement, and start of forward buccal mass movement to peak protraction) are indicated by shaded regions. Data have been smoothed *via* running average with a window size of five points (1/3 s total).

eccentricity, measured from lateral-view tracings of transilluminated slugs, quantify the dimensional changes of the buccal mass during sequential swallows (Fig. 6). These plots make it possible to characterize buccal mass shapes intermediate between full protraction, transition or full retraction, i.e. intermediate between shapes 1, 2 and 3. In general, ellipticity is nearest zero (most round) at the peaks of protraction and retraction, and most negative (most elongated along the antero-posterior axis) during the first third of retraction (*t1*) and at the start of the second half of protraction. Eccentricity is also maximal (greatest asymmetry) at the peak of retraction, with a variable minor peak during stable transition (*t3*) or protraction; minimum eccentricity (greatest symmetry) corresponds to the peak of protraction. Peaks of ellipticity occur at twice the frequency of peaks of eccentricity; the implications of this correspondence are considered in the Discussion.

Plots of eccentricity *versus* ellipticity show the progression of the buccal mass through shape space during swallowing (Fig. 7A–I). Most of the nine sequential swallows presented follow a closed-loop, C-shaped or L-shaped path. In all cases, however, the qualitatively defined shape classes shape 1 (spherical), shape 2 (ovoid) and shape 3 (Γ-shaped) occupy separate regions in the quantitative shape space. Additionally, key buccal mass movements, determined independently of shape space measurements, correspond to points of local maximum extent into these different shape space regions. In general, the peaks of protraction and retraction and the stable transition occur at the extremes of the C-shaped or L-shaped paths through shape space.

Hysteresis

Most of the swallows show paths from shape 2 to shape 3 through shape space that are distinctly different from the paths from shape 3 to shape 2, or hysteresis (Fig. 7A,C–G). Moreover, the hysteresis takes two different forms. In the first

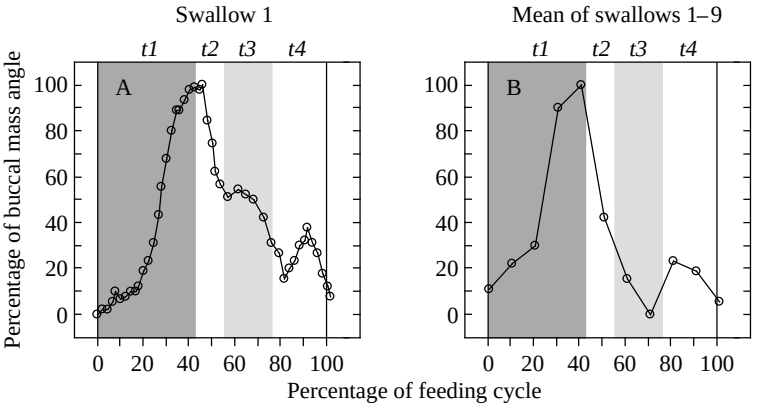

Fig. 5. Plots of buccal mass angle *versus* time, normalized to percentages (0%=minimum, 100%=maximum). (A) Swallow 1 (a pure swallow). (B) Mean of all normalized swallows 1–9 (pure swallows and swallows/tears/head flexion). Note the absence of a peak during *t3* compared with A. Data have been smoothed *via* running average with a window size of five points (1/3 s total).

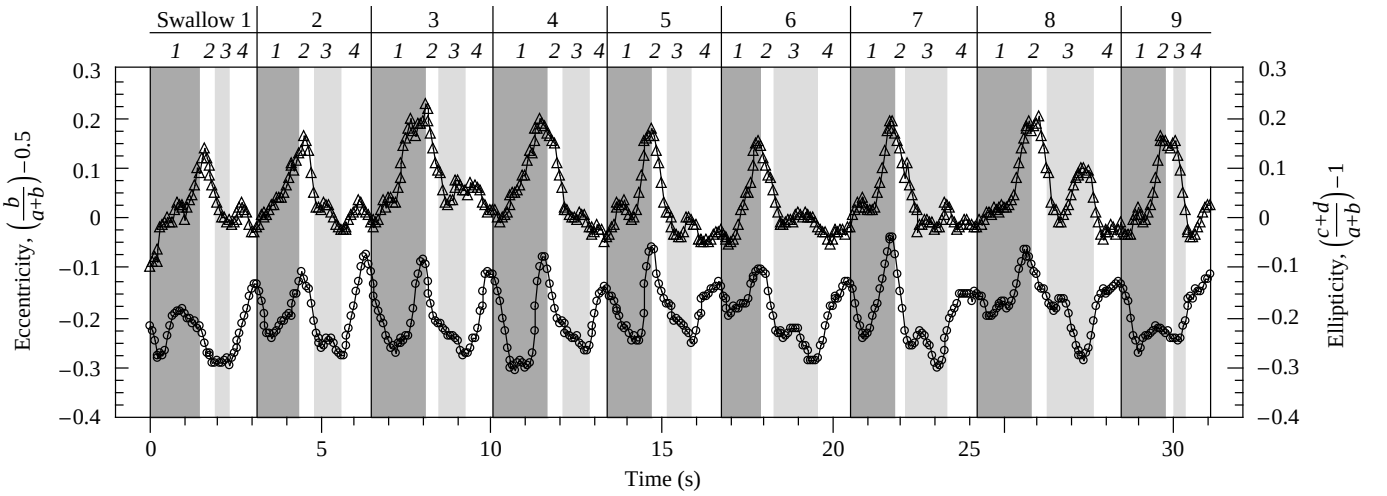

Fig. 6. Plot of eccentricity (triangles, top) and ellipticity (circles, bottom) *versus* time for nine consecutive swallows. Swallows and *t1–t4* intervals are indicated by lines and shaded regions as in Fig. 4. Data have been smoothed *via* running average with a window size of five points (1/3 s total).

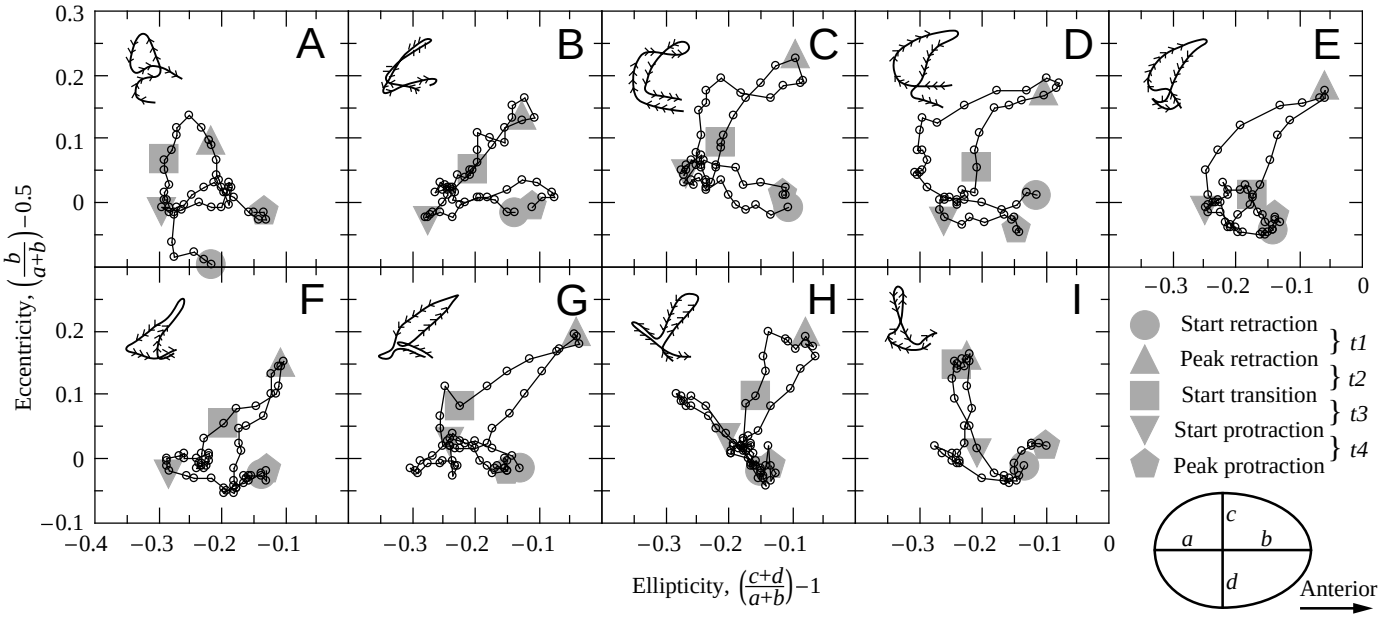

Fig. 7. (A–I) Shape space plots of eccentricity *versus* ellipticity for nine consecutive swallows from full protraction to full protraction. Each point represents 1/15 s. The peaks of protraction and retraction and the beginnings of stable transition and the second half of protraction are highlighted for each swallow, to facilitate comparison among swallows. Data have been smoothed *via* running average with a window size of five points (1/3 s total). Insets show the direction of each path through shape space. For details, see Results.

hysteresis pattern, seen in swallows 3, 4 and 5, the path leading into shape 3 (the latter half of *t1*) has more negative ellipticity (shapes are more elliptical along the antero-posterior axis and less round) than the path leading from shape 3 into shape 2 (*t2* and the start of *t3*) (Fig. 7C–E). The second hysteresis pattern, seen in swallows 6, 7 and 8, shows the reverse: the path leading into shape 3 has less negative ellipticity (shapes are rounder) than the path leading from shape 3 into shape 2 (Fig. 7F–H). Hysteresis is not present in swallows 2 and 9; the paths through shape space to and from shape 3 are mostly identical (Fig. 7B,I). It is interesting that the swallows showing the first hysteresis pattern are mostly pure swallows (three out of five, counting swallow 5 as a transitional response), while those showing the second pattern are mixed swallows/tears (three out of four).

Variability

The time plots of ellipticity and eccentricity (Fig. 6) show local variations in the general patterns described above. For example, eccentricity for swallow 1 during the peak

protraction to peak retraction interval (*t1*) is different from that for all other swallows; buccal mass shapes here are skewed posteriorly instead of anteriorly as elsewhere. Ellipticity and eccentricity change according to the same regular pattern from the stable transition period of swallow 1 (*t3*) to the peak protraction at the start of swallow 5. Thereafter, the time plots of ellipticity and eccentricity begin to show irregularities, which become pronounced during swallows 8 and 9. A minor extra peak of eccentricity appears in *t1* of swallow 5; a large extra peak is seen in *t3* of swallow 8. The local minima of ellipticity are not consistently at the previous baseline levels beginning in swallow 6, and the local maxima are not of consistent height.

The shape space plots (Fig. 7) magnify these variations and irregularities. The retraction phase (*t1*) of swallow 1 follows a unique shape space path (Fig. 7A). Instead of a single arc from peak protraction to peak retraction, a tortuous curve is seen in swallow 5 (Fig. 7E). The stable transition shapes of swallow 7 (Fig. 7G) and, more markedly, swallow 8 (Fig. 7H) are characterized by abrupt 'detours' in shape space: whereas stable transition shapes (*t3*) of other swallows are less elliptical than the start of protraction (*t3*/*t4* boundary), in swallows 7 and 8 the stable transition shapes are more elliptical. In swallows 7, 8 and 9 (Figs 7G–I), the starts of protraction are also not at points of local maximum extent; they are less elliptical than the local maxima. The shape space region containing peak retraction shapes in swallow 9 (Fig. 7I), while separate from the protraction and transition regions in this swallow, is not the same region as the peak retraction shapes in swallows 2–8 (Fig. 7B–H).

Normalized dimensional changes

To determine whether there was an average kinematic pattern for the buccal mass during the nine swallows studied, despite the variability observed, a shape space analysis was performed on a normalized data set (Fig. 8). As in the normalization of buccal mass angle data, the *t1–t4* timebase intervals of each swallow were normalized to the mean *t1–t4* intervals. Dimension measurements *a*, *b*, *c* and *d* were sorted into 1/3 s bins, and the ellipticity and eccentricity parameters were calculated from the means of the bins. The normalized buccal mass has its maximum antero-posterior and dorso-ventral lengths during full retraction (Fig. 8A,B), corresponding to the *in vivo* Γ-shape seen in Fig. 3A. Note that the shape space treatment of the buccal mass as ellipse quadrants does not capture the antero-ventral constriction observed around full retraction (Fig. 8D, 4–6). The minimum antero-posterior and dorso-ventral lengths occur at full

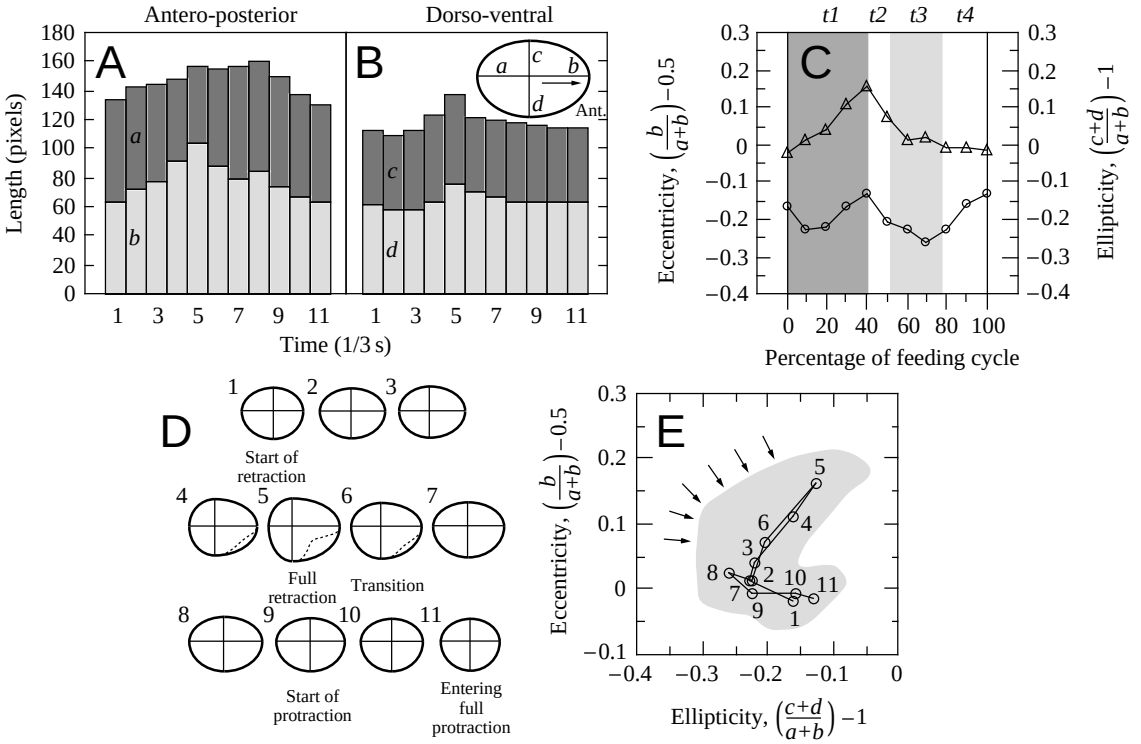

Fig. 8. Mean shape space data for swallows 1–9, with time normalized to mean *t1–t4* times. (A) Mean changes in *a* and *b* buccal mass measurements. (B) Mean changes in *c* and *d* buccal mass measurements. (C) Mean eccentricity (triangles, top) and ellipticity (circles, bottom), normalized to percentage of the feeding cycle. (D) Ellipse quadrant buccal mass representations implied by the mean *a*, *b*, *c* and *d* values in 1/3 s intervals. Note that the antero-ventral concavity seen *in vivo* during 4–6 is not accurately represented. (E) Mean shape space plot. Numbered points represent the numbered shapes in D. The gray region is the range of variability for the original nine swallows (unaveraged). Note that, in contrast to most of the individual shape space plots shown in Fig. 7, there is no hysteresis seen in the mean shape space plot. Arrows highlight the particularly large variability in the individual shape 2 → shape 3 and shape 3 → shape 2 paths *in vivo* compared with the mean paths.

protraction (Fig. 8A,B), corresponding to the *in vivo* rounded shape seen in Fig. 3C.

Of the shape parameters, ellipticity shows maxima (greatest circularity) at peak protraction and peak retraction, and minima (greatest antero-posterior extent) in mid-*t1* and mid-*t3* (Fig. 8C). Eccentricity shows a single maximum at peak retraction, with a plateau at the minimum throughout *t3* and *t4* (Fig. 8C). In the shape space plot of normalized eccentricity *versus* normalized ellipticity (Fig. 8E), the behavioral extremes of full protraction, full retraction and transition occupy separate regions of shape space, just as in most of the individual swallows (Fig. 7). At full protraction, the buccal mass is relatively circular and symmetrical. At full retraction, it is equally circular but also eccentric (skewed posteriorly). During the stable post-retraction transition, the buccal mass is symmetrical but elliptical along the antero-posterior axis. An unexpected result is that, while seven of the nine swallows display hysteresis in their individual shape space plots, the normalized shape space plot has none: the path from peak protraction to peak retraction (i.e. radular retraction) is identical to the path from peak retraction to peak protraction (i.e. radular protraction). The significance of this discrepancy is considered in the Discussion.

Discussion

We have characterized the kinematics of the buccal mass of *Aplysia californica* during swallowing cycles (and cycles of mixed swallows/tears) *in vivo*, using intact, transilluminated juveniles. At different phases of the feeding cycle (full protraction, transition, full retraction), the buccal mass assumes characteristic shapes (spherical, ovoid, Γ-shaped); it also undergoes distinct rotational movements which peak during retraction. The kinematics allows the timing of different phases of the feeding cycle to be determined. As the buccal mass changes shape, however, intermediate shapes arise which cannot be unambiguously assigned to a qualitative shape class. The transitions between shape classes can be accurately quantified using two measurable shape parameters, ellipticity and eccentricity, which together form a two-dimensional shape space. The path traversed by the buccal mass through this shape space is a reflection of the anatomical and biomechanical changes that occur at every point in the feeding cycle. Shape space analysis is robust enough to demonstrate a common kinematic pattern for the nine consecutive swallows studied, yet sensitive enough to distinguish pure swallows (swallows 1–4) from swallows/tears (swallows 5–9), by demonstrating tendencies to different forms of hysteresis to and from peak retraction in the shape space paths.

Generality of results

We are confident that the presented sequence of nine consecutive swallows is typical of swallowing (and tearing) behavior in *A. californica*. The analyzed sequence of nine consecutive swallows is the best-controlled sample in our entire collection of recorded feeding sequences from over 30 slugs. We have observed many swallowing sequences with lesser control of parallax (in both one-axis and two-axis video arrangements) which are qualitatively identical to the data shown in Fig. 3. Indeed, a preliminary, manually measured version of the shape space analysis was performed upon the 'best' one-axis feeding sequence, with results similar to those presented (data not shown). Our analysis is strengthened, however, by having used a data set in which it could be clearly demonstrated that there were no parallax difficulties.

One limitation of these results is that we have not studied the shape changes that occur in adult *A. californica in vivo*, and it is possible that these shapes might differ from those of juveniles. However, studies of dissected innervated adult buccal masses induced to generate feeding-like movements by applying electric shocks to the buccal ganglia nerves indicate that the shapes produced by adult buccal masses under these circumstances are very similar to those that we observed in juvenile *A. californica in vivo*.

Buccal mass shape changes

The buccal mass shapes we observed in transilluminated juvenile *A. californica* more closely resemble those observed in the *Lymnaea stagnalis* buccal mass *in vitro* (Rose and Benjamin, 1979) than those predicted for *A. californica* on the basis of a feeding head preparation by Weiss *et al.* (1986). The most striking similarity between *Aplysia* and *Lymnaea* buccal mass shapes is in full retraction: both have a Γ-shaped buccal mass with a ventral projection and an antero-ventral concavity. The shape of the buccal mass during full retraction proposed by Weiss *et al.* (1986) shows an oval shape lacking an antero-ventral concavity. The full protraction (and transition) shapes in *Lymnaea* are roughly oval, whereas we observed clearly different shapes for these phases of the feeding cycle in *A. californica:* the buccal mass shape at full protraction is nearly spherical, whereas the buccal mass shape at transition is ovoid. A distinctly rounded shape is predicted by Weiss *et al.* (1986) for the extreme protraction of a bite–swallow cycle. This shape is smaller than that observed in swallow and tear/swallow cycles in the present study (in which the radula did not protract through the jaws). Indeed, the shape of the buccal mass in full protraction proposed by Weiss *et al.* (1986) appears compressed so that it is taller (dorso-ventral axis) than it is wide (antero-posterior axis). The oval transition shapes observed in *Lymnaea* are similar to our observations in transilluminated juvenile *A. californica* and to the 'rest' shape predicted by Weiss *et al.* (1986).

Buccal mass angular changes

In addition to internal shape changes, the *A. californica* buccal mass undergoes approximately 10 ° of dorsal rotation during the retraction phase and rotates back to its original position during protraction (Fig. 4). The anatomy of the extrinsic muscles suggests that they might be responsible for the rotation (Howells, 1942; Chiel *et al.* 1986). Fig. 9 shows a schematic correlation of changes in buccal mass angle during an average pure swallow with typical EMG recordings from

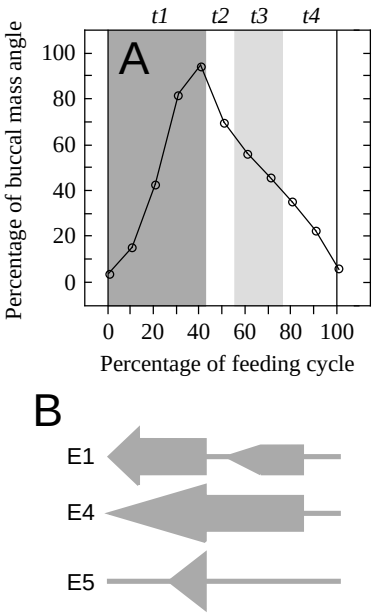

Fig. 9. Schematic correlation of buccal mass angle changes in pure swallows with electromyographic (EMG) activity in extrinsic muscles E1, E4 and E5 over one feeding cycle. Buccal mass angles are the means of normalized swallows 1–4. EMG data are derived from Chiel *et al.* (1986) by rescaling the individual timebases to a single feeding cycle length.

the E1, E4 and E5 muscles (EMG data modified from Chiel *et al.* 1986). Since the EMG recordings were scaled only by cycle time, the parts of each recording that correspond to the intervals *t1–t4* cannot be precisely determined, but some trends seem clear. E1, E4 and E5 all appear to be active during the retraction phase, but with different patterns of activation: E1 is active throughout, but most active initially; E4 activity increases throughout to a maximum at what appears to be peak retraction; E5 is active only during the end of the retraction phase, its activity also seeming to peak at full retraction. While E1 and E4 show subsequent activities, E5 is inactive for the remainder of the feeding cycle. Although these data are pooled and do not represent simultaneous recordings from single individuals, they nevertheless suggest that some extrinsic muscles are active at functionally different points in the feeding cycle, especially during retraction. Experimental lesions of all of the extrinsic muscles lead to deficits in swallowing; this is likely to be due to deficits in retraction, since protraction movements appear normal in lesioned slugs (Chiel *et al.* 1986).

Shape space analysis

The parameters ellipticity and eccentricity capture functionally relevant dimensional changes in *A. californica* buccal mass shape during the feeding cycle (Fig. 6). Plots of eccentricity *versus* ellipticity form a two-dimensional shape space in which the distinctive buccal mass shapes observed at full protraction, full retraction and transition occupy distinct regions, and the progress through the feeding cycle is translated into movement through the space (Fig. 7). The validity of the method is demonstrated by the fact that the points of maximal extent into different regions of shape space correspond to the extremes of behavior as determined by other means (e.g. peaks of protraction and retraction from movement of the buccal mass, buccal mass angle changes).

Uniqueness of shape space parameters

Because the ellipticity and eccentricity parameters are ratios of sums, many ‘different’ shapes can share a given parameter value. For example, the time plot of ellipticity shows two peaks (of similar value) per feeding cycle: one at peak protraction, the other at peak retraction (Fig. 6). The buccal mass shapes at these points, however, are absolutely different (compare Fig. 3A with Fig. 3C). Ellipticity fails to distinguish these shapes because it is sensitive only to the ratio of the antero-posterior and dorso-ventral lengths, not to their asymmetries (insets to Fig. 3G,I; note the similarity in the relative sizes of the axes). While none is observed in the data, ‘different’ shapes which nonetheless have identical eccentricity parameters can also exist.

When ellipticity and eccentricity parameters are combined in a shape space plot, however, discrimination is markedly increased. For example, although peak protraction and peak retraction have similar ellipticity, they have markedly different eccentricity: low at peak protraction and high at peak retraction. The result is that the peak protraction and peak retraction shapes occupy different regions in the two-dimensional shape space (Fig. 8E, compare points 1 and 5). Given the range of buccal mass shape changes observed *in vivo*, the probability is low that ‘different’ shapes will share *both* ellipticity and eccentricity parameter values, and thus map to the same region of shape space. It is also unlikely that ‘similar’ buccal mass shapes will have such different shape parameters that they map to different regions of shape space. Shape space analysis is not unique, but it is ‘unique enough’ to discriminate the shapes of interest.

In general, the shape space analysis that we have described in this paper may be of use for discriminating between planar convex shapes with two axes of symmetry, both of which can vary independently in size and one of which can vary in location relative to the midpoint of the other axis. However, as shown in Fig. 8D parts 4–6, this analysis cannot effectively distinguish concavities that may develop in the planar shape. It would be possible to add another variable to describe this particular concavity, but the analysis would then require three dimensions. The approach we have taken could be generalized to deal with more axes of symmetry and further irregularities. The aspect of shape space analysis that is likely to be of general use, however, is the method of approach: recognizing that there are specific constraints on the shapes assumed by the particular structure of interest and capturing these constraints as simply as possible.

Variability between swallows

Because of our confidence in the sensitivity of shape space

analysis, we believe that the differences observed in the shape space plots of swallows 1–4 and swallows 5–9 are not due to experimental error. Instead, this variability is likely to be evidence of functional adaptation in *A. californica* feeding behavior. In the first four swallows, the seaweed is simply being pulled into the buccal cavity, with little apparent resistance. At the end of the fourth swallow, the leading end of the seaweed has reached the posterior buccal cavity and is pushing against the junction of the esophagus. The five subsequent swallows actually include sharp rasping movements of the radula/odontophore, which break off pieces of seaweed in addition to drawing it further into the mouth. The handling characteristics of the food are clearly changing during these five swallows, and this is reflected in the shape space plots.

Hysteresis and 'active' and 'return' phases

The shape space plots of many of the nine consecutive swallows studied show hysteresis: the path shape 1 → shape 2 → shape 3 is not the same as the path shape 3 → shape 2 → shape 1 (e.g. Fig. 7D). Indeed, two different forms of hysteresis were observed, one occurring during pure swallows, the other during swallows with tearing behavior (Fig. 7; see Results). Weiss *et al.* (1986) proposed that, on the basis of variable timing, protraction and retraction each had an 'active' phase and a 'return' phase, each possibly under control of a different oscillator. The movements themselves, however, they hypothesized to be symmetrical (i.e. one would be the exact reverse of the other; presumably, this would also apply to movement in shape space). Our data support such distinctions within the protraction and retraction phases. In this sequence of nine consecutive swallows, however, we find (a) that feeding cycle timing is rather constant, even to the intervals *t1–t4* (Table 1); and (b) that the movements to and fro are mostly different, as shown by hysteresis in the individual shape space plots (Fig. 7). Interestingly, the average shape space plot for all nine swallows shows no hysteresis (Fig. 8E). This is probably because, in aggregate, all the individual hysteresis paths cancel out: some have the transition to peak retraction path more elliptical than the peak retraction to transition path, some have the reverse, and the rest (the minority) have no hysteresis (Fig. 7).

We would prefer a more neutral nomenclature than 'active' and 'return' phases, since the latter implies a passive mechanism such as simple relaxation (although Weiss *et al.* 1986, never use the term 'passive'). It is possible that both phases are 'active' in the sense of requiring specific muscle contraction(s) in order to occur. We are hesitant, however, to propose an alternative nomenclature, since the anatomical, functional and neural bases of the hysteresis are still unknown.

Another interesting feature of our results is the distinction between stable and dynamics transitions (i.e. the path taken through shape 2). During the swallows and swallow/tears that we observed, the movement from peak protraction to peak retraction involved continuous, dynamic changes in the shape of the buccal mass. In contrast, after peak retraction, there was a period during which the buccal mass assumed a relatively stable ovoid shape, and this period of stable transition (*t3*) persisted for an average of about one-quarter of each swallow cycle (Table 1). The stable transition may correspond to an inter-swallow interval, suggesting that the pattern generator could produce a protraction and then a retraction movement in each behavioral response, followed by a variable interval during which no overt movement is produced. To solve this problem conclusively would require further studies of other behavioral responses, especially rejection, in which protraction, rather than retraction, is the power stroke of the behavior.

Implications for internal structure and function of the buccal mass

Published observations of the buccal mass from other molluscs serve as a basis for informed speculation about the functions of analogous components in *A. californica*. The overall buccal mass shape, whether *in vivo* or *in vitro*, is determined by anatomy (origins and insertions of muscles, shapes and relationships of components) and by functional properties (patterns of muscle contraction, muscle biomechanics). The shape, and the changes in shape, thus provide important information about the internal structure and function of the buccal mass. Because of similarities in anatomy, the large volume occupied by the radula/odontophore and the cartilaginous structures within the odontophore, it is possible that similar buccal mass kinematics in different species of mollusc (such as *Aplysia* and *Lymnaea*) may reflect fundamentally similar mechanisms of action of the buccal mass.

However, results derived from isolated buccal masses, both spontaneously contracting (Rose and Benjamin, 1979) and electrically stimulated (Herrick, 1906), feeding head preparations (Weiss *et al.* 1986) or fixed specimens (MacFarland, 1924; Rose, 1971; Smith, 1990) must be treated with caution. For example, Rose and Benjamin (1979) noted that bite–swallows did not appear spontaneously in isolated *Lymnaea stagnalis* buccal masses, so it is possible that the lack of more spherical peak protraction shapes in their study is an artifact of isolation and the absence of normal hydrostatic pressure. Also, in many (especially older) studies, clear distinctions are not drawn between what was observed *in vivo*, *in vitro* and from dissections. We believe, however, that we have not drawn unreasonable inferences for *Aplysia* from the molluscan literature.

Mechanism of protraction and retraction

Protraction and retraction in *A. californica* may be achieved through mechanisms similar to those described in other molluscs. For example, in *Lymnaea stagnalis*, the anterior and posterior jugalis muscles are active (as measured by EMG) during protraction and retraction, respectively (Rose and Benjamin, 1979). By anatomical criteria, the analogs to these muscles in *Aplysia* are I2 and I1/I3, respectively (Howells, 1942; Scott *et al.* 1991; Hurwitz *et al.* 1996). Contraction of

I2 is likely to assist in protraction: anatomically, it might cause a general foreshortening and rounding of the buccal mass and/or help the radula/odontophore to rotate forward. Hurwitz *et al.* (1996) have shown that I2 has EMG activity during protraction, and lesions of I2 prevent full protraction of the radula/odontophore during bite–swallows; however, normal rotation of the radula is still visible through the open jaws. This suggests that 'protraction' has separate rotational and translational components, and that I2 function is important for translation (i.e. anterior movement of the entire buccal mass). Contraction of I1/I3 is likely to force the radula/odontophore posteriorly and cause the antero-ventral concavity observed in the buccal mass during retraction (Fig. 3A,G). This could also produce the ventral extension of the radular stalk (see below), but internal odontophore muscles could also be responsible. On the basis of anatomy, other species of mollusc with muscles in arrangements similar to the anterior-posterior jugalis and I2–I1/I3, such as *Hancockia californica* (MacFarland, 1924), *Archidoris pseudoargus* (Rose, 1971) and *Helisoma trivolvis* (Kater, 1974; Smith, 1990), may undergo buccal mass shape changes during their feeding cycles similar to those in *Lymnaea* and *Aplysia*.

Radula/odontophore movements and shape changes

Historically, it has been a point of contention in the molluscan literature as to whether the radula is capable of significant movement, independent of the underlying ondontophore 'cartilages' or bolsters, in particular species or as a general mechanism of molluscan feeding (for a review, see Smith, 1988). In *Helisoma*, the radula can clearly be protracted and retracted separately from the protraction and retraction of the odontophore (Smith, 1988), whereas in *Archidoris*, the radula and odontophore are closely joined and usually move together as a unit (Rose, 1971). The odontophore in *Aplysia* is mostly muscle (I4), with small bolsters deeply embedded therein (Eales, 1921; Starmühlner, 1956; Drushel *et al.* 1993), suggesting that there is little movement between radula and odontophore. The fact that *Aplysia* feeds by biting (Howells, 1942; Kupfermann, 1974) rather than by rasping is also consistent with this idea, and Weiss *et al.* (1986) depict a static radula/odontophore in their description of possible buccal mass shape changes.

Our kinematic study of the *A. californica* buccal mass, however, strongly suggests that the radula/odontophore changes shape during the feeding cycle (Fig. 10). The prominent ventral projection seen in the Γ-shape that occurs at full retraction must be due to the radular stalk (which is continuous topologically with the radular surface). By analogy with *Lymnaea stagnalis* (Rose and Benjamin, 1979), the radular stalk is probably nearly perpendicular to the antero-posterior axis of the buccal mass (not inclined posteriorly at 45° as proposed by Weiss *et al.* 1986) and somewhat lengthened. For the radula and odontophore to fit within the observed *in vivo* buccal mass outline, the radular surface must tilt posteriorly (increasing the angle with the radular stalk) and the cleft between the radular halves must deepen (allowing the radular stalk to lengthen) (Fig. 10A). During transition and 'rest', the radula and odontophore are substantially as predicted by Weiss *et al.* (1986) (Fig. 10B). The protraction of swallowing requires forward rotation of the *radula/odontophore*, but not such extreme rotation that the radula protrudes through the jaws (Fig. 10C). In the full

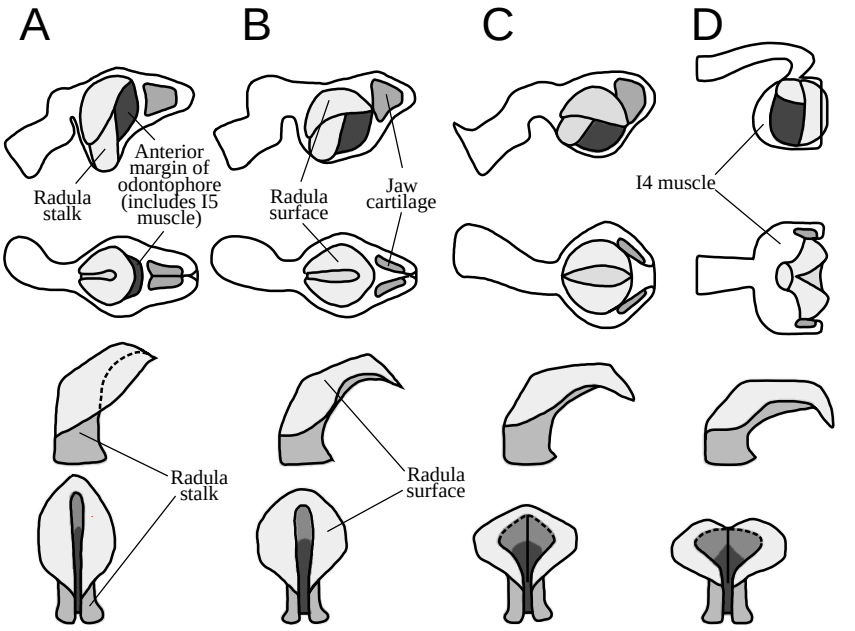

Fig. 10. Schematic prediction of the shape and position of the radular surface, radular stalk and jaw cartilages inside the buccal mass during the feeding cycle, as seen in lateral (top row) and dorsal (second row) views, using *in vivo* kinematics as constraints. Buccal mass outlines in A–C are based upon Fig. 3G–L, rotated such that the buccal mass angle is 0°. The outlines in D are based on careful examinations of the few bites that were observed in transilluminated animals. The internal structures shown are constrained to fit within the buccal mass outlines. Detailed predictions for the radular surface and radular stalk are shown in lateral (third row) and posterior (fourth row) views, based upon isolated radulas prepared by maceration of both fresh and formalin-fixed buccal masses with 5.0 mol l^{-1} KOH (not to the same scale as the top two rows). The radular surface/stalk must change shape with a constant surface area, since they are topologically a continuous sheet of inelastic tissue. For details, see Discussion. (A) Swallow peak retraction. (B) Stable transition. (C) Swallow peak protraction. (D) Bite peak protraction. Note that, in order to present the entire dorsal surface of the radula through the jaws, the entire buccal mass has been rotated approximately 45° forwards, independent of the 45° internal forward rotation of the radula/odontophore. Protraction shapes with the forward-stretched esophagus were actually observed in one transilluminated animal (one-axis view) during tearing upon large, intact stipes of *Gracilaria* sp. (data not shown).

protraction of a bite–swallow, however, the entire dorsal surface of the radula is visible through the open jaws (Kupfermann, 1974). To maintain a fixed radula/odontophore, however, would require that the entire structure undergo an internal 90 ° rotation (relative to the rest of the buccal mass) to present the radula as observed (Weiss *et al.* 1986). On the basis of our anatomical studies of dissected buccal masses, this would be extremely unlikely to occur. The difficulty seems to us easily resolved if (a) the radula/odontophore internally rotates 45 ° forward, as in a swallow protraction; (b) the radular surface flattens anteriorly, decreasing the angle with the radular stalk; (c) the radular stalk shortens as the radular surface flattens; and (d) the entire buccal mass is foreshortened and rotated forward by 45 °, stretching the esophagus and gut anteriorly (Fig. 10D). The I2 and extrinsic muscles are probably responsible for the foreshortening and rotation of the buccal mass, respectively. Also, the proposed peak protraction shape of Weiss *et al.* (1986) appears compressed so that it is taller (dorso-ventral axis) than it is long (antero-posterior axis). Assuming that the buccal mass must change shape isovolumetrically (owing to the incompressibility of water in muscle and bolsters), this shape must correspondingly be very wide in the medio-lateral axis. We did observe dimensional changes in this direction in dorsal view (Fig. 3F,L), but not to such a large extent, and we believe that the magnitude of change required would be unlikely given the anatomy.

On the basis of our observations, we hypothesize that there are two physical constraints on the shape changes of the radula/odontophore: (a) the shape changes are isovolumetric for the radula/odontophore; and (b) the surface area of the radular surface and stalk are constant.

Implications for modeling studies

Using the observed kinematics of swallowing as constraints, we can predict the positions and movements of internal structures in the *A. californica* buccal mass which cannot be observed directly. A qualitative prediction of radula/odontophore shapes and movements is already possible (Fig. 10). More accurate predictions can be made by developing a quantitative kinematic model of the buccal mass, in which important structural elements (muscles, radula, odontophore) are represented, with correct anatomical relationships, and allowed to move and change dimensions according to defined rules (such as isovolumetricity for muscles). Shape space analysis provides a method of testing the validity of the model output: models which produce shape space plots similar to those observed *in vivo* are 'better' than those that do not. An analytical kinematic model of the feeding cycle in *Aplysia californica* has already appeared in preliminary form (Neustadter *et al.* 1992) and, by using shape space analysis as a selection tool, we have subsequently developed a more complex and accurate version (Drushel *et al.* 1994; R. F. Drushel, D. M. Neustadter, P. E. Crago and H. J. Chiel, in preparation).

Modeling constrained by *in vivo* kinematics is a powerful tool for investigating feeding behavior. Kinematic models can predict muscle lengths, allowing predictions of muscle action and patterns of muscle activity. Kinetic models with proper kinematics can test hypotheses about muscle forces and biomechanics. Ultimately, models of neural control can be applied to kinetic models, creating a complete model of the buccal mass. At every step, appropriate *in vitro* tests can be performed to verify the predictions of the models; but every model must be constrained by the fundamental requirement that it reproduce the *in vivo* kinematics.

The present kinematic analysis of feeding in *A. californica* reflects our philosophy that it is valid to characterize the periphery and use knowledge of its properties to work backwards towards neural control. This method is intended to complement the more standard procedure of first characterizing the neural control and then attempting to understand the periphery. We believe that both methods are useful and, in fact, necessary for the study of the neural basis of behavior.

We thank Christopher A. Elkins for assistance with creating QuickTime movies from hundreds of PICT images. This work was supported by NIH grant HL-25830.

References

ARSHAVSKY, Y. I., DELIAGINA, T. G., MEIZEROV, E. S., ORLOVSKY, G. N. AND PANCHIN, Y. V. (1989*a*). Control of feeding movements in the freshwater snail *Planorbis corneus*. III. Organization of the feeding rhythm generator. *Expl Brain Res.* **70**, 332–341.

ARSHAVSKY, Y. I., DELIAGINA, T. G., ORLOVSKY, G. N. AND PANCHIN, Y. V. (1989*b*). Control of feeding movements in the pteropod mollusc, *Clione limacina*. *Expl Brain Res.* **78**, 387–397.

BENJAMIN, P. R. AND ELLIOTT, C. J. H. (1989). Snail feeding oscillator: The central pattern generator and its control by modulatory interneurons. In *Neuronal and Cellular Oscillators* (ed. J. W. Jacklet), pp. 173–213. New York: Marcel Dekker, Inc.

BIZZI, E., MUSSA-IVALDI, F. AND GISZTER, S. (1991). Computations underlying the execution of movement: a biological perspective. *Science* **253**, 287–291.

BULLOCH, A. G. M. AND RIDGWAY, R. L. (1995). Comparative aspects of gastropod neurobiology. In *The Nervous Systems of Invertebrates: An Evolutionary and Comparative Approach* (ed. O. Breidbach and W. Kutsch), pp. 89–113. Basel, Switzerland: Birkhauser Verlag.

CARRIKER, M. R. (1946). Observations on the functioning of the alimentary system of the snail *Lymnaea stagnalis appressa* Say. *Biol. Bull. mar. biol. Lab., Woods Hole* **91**, 88–111.

CHIEL, H. J. AND BEER, R. D. (1993). Neural and peripheral dynamics as determinants of patterned motor behavior. In *The Neurobiology of Neural Networks* (ed. D. Gardner), pp. 137–164. Cambridge, MA: The MIT Press.

CHIEL, H. J. AND SUSSWEIN, A. J. (1993). Learning that food is inedible in freely-behaving *Aplysia californica*. *Behav. Neurosci.* **107**, 327–338.

CHIEL, H. J., WEISS, K. R. AND KUPFERMANN, I. (1986). An identified histaminergic neuron modulates feeding motor circuitry in *Aplysia*. *J. Neurosci.* **6**, 2427–2450.

CHIRIKJIAN, G. S. AND BURDICK, J. W. (1995*a*). The kinematics of

hyper-redundant robot locomotion. *IEEE Trans. Robotics Automation* **11**, 781–793.

CHIRIKJIAN, G. S. AND BURDICK, J. W. (1995*b*). Kinematically optimal hyper-redundant manipulator configurations. *IEEE Trans. Robotics Automation* **11**, 794–806.

CROLL, R. P., DAVIS, W. J. AND KOVAC, M. P. (1985). Neural mechanisms of motor program switching in the mollusc *Pleurobranchaea*. I. Central motor programs underlying ingestion, egestion and the 'neutral' rhythm(s). *J. Neurosci.* **5**, 48–55.

DELANEY, K. AND GELPERIN, A. (1990). Cerebral interneurons controlling fictive feeding in *Limax maximus*. II. Initiation and modulation of fictive feeding. *J. comp. Physiol.* **166**, 311–326.

DRUSHEL, R. F., CRAGO, P. E. AND CHIEL, H. J. (1993). The muscular hydrostatic structure of the buccal mass of *Aplysia californica.* Abstract 657.1. 23rd Annual Meeting, Society for Neuroscience.

DRUSHEL, R. F., CRAGO, P. E. AND CHIEL, H. J. (1994). Static- and dynamic-radula/odontophore kinematic models of the buccal mass of *Aplysia californica.* Abstract 653.19. 24th Annual Meeting, Society for Neuroscience.

EALES, N. B. (1921). *Aplysia.* LMBC Memoir XXIV. Liverpool: Liverpool University Press. 84pp.

HERRICK, J. C. (1906). Mechanism of the odontophoral apparatus in *Sycotypus canaliculatus. Am. Nat.* **40**, 707–737.

HOWELLS, H. H. (1942). The structure and function of the alimentary canal of *Aplysia punctata. Q. Jl microsc. Sci.* **83**, 357–397.

HURWITZ, I., GOLDSTEIN, R. S. AND SUSSWEIN, A. J. (1994). Compartmentalization of pattern-initiation and motor functions in the B31 and B32 neurons of the buccal ganglia of *Aplysia californica*. *J. Neurophysiol.* **71**, 1514–1527.

HURWITZ, I., NEUSTADTER, D., MORTON, D. W., CHIEL, H. J. AND SUSSWEIN, A. J. (1996). Activity patterns of the B31/B32 pattern initiators innervating the I2 muscle of the buccal mass during normal feeding movements in *Aplysia californica. J. Neurophysiol.* **75**, 1309–1326.

HURWITZ, I. AND SUSSWEIN, A. J. (1992). Adaptation of feeding sequences in *Aplysia oculifera* to changes in load and width. *J. exp. Biol.* **166**, 215–235.

KATER, S. B. (1974). Feeding in *Helisoma trivolvis:* The morphological and physiological bases of a fixed action pattern. *Am. Zool.* **14**, 1017–1036.

KATZ, P. S. AND FROST, W. N. (1996). Intrinsic neuromodulation: altering neuronal circuits from within. *Trends Neurosci.* **19**, 54–61.

KIER, W. M. AND SMITH, K. K. (1985). Tongues, tentacles and trunks: The biomechanics of movement in muscular-hydrostats. *Zool. J. Linn. Soc.* **83**, 307–324.

KUPFERMANN, I. (1974). Feeding behavior in *Aplysia:* A simple system for the study of motivation. *Behav. Biol.* **10**, 1–26.

MACFARLAND, F. M. (1924). The morphology of the nudibranch genus *Hancockia. J. Morph.* **38**, 65–104.

MORTON, D. W. AND CHIEL, H. J. (1993*a*). *In vivo* buccal nerve activity that distinguishes ingestion from rejection can be used to predict behavioral transitions in *Aplysia*. *J. comp. Physiol.* A **172**, 17–32.

MORTON, D. W. AND CHIEL, H. J. (1993*b*). The timing of activity in motor neurons that produce radula movements distinguishes ingestion from rejection in *Aplysia*. *J. comp. Physiol.* A **173**, 519–536.

NEUSTADTER, D., CHIEL, H. J., CRAGO, P. E., MANSOUR, J. M. AND BEER, R. D. (1992). A kinematic model of the buccal mass of *Aplysia.* **Abstract 190**. Third International Congress of Neuroethology.

QUINLAN, E. M., GREGORY, K. AND MURPHY, A. D. (1995). An identified glutaminergic interneuron patterns feeding motor activity *via* both excitation and inhibition. *J. Neurophysiol.* **73**, 945–956.

ROSE, R. M. (1971). Functional morphology of the buccal mass of the nudibranch *Archidoris pseudoargus. J. Zool., Lond.* **165**, 317–336.

ROSE, R. M. AND BENJAMIN, P. R. (1979). The relationship of the central motor pattern to the feeding cycle of *Lymnaea stagnalis. J. exp. Biol.* **80**, 137–163.

SCOTT, M. L., GOVIND, C. K. AND KIRK, M. D. (1991). Neuromuscular organization of the buccal system in *Aplysia californica. J. comp. Neurol.* **312**, 207–222.

SMITH, D. A. (1988). Radular kinetics during grazing in *Helisoma trivolvis* (Gastropoda: Pulmonata). *J. exp. Biol.* **136**, 89–102.

SMITH, D. A. (1990). Comparative buccal anatomy in *Helisoma* (Mollusca, Pulmonata, Basommatophora). *J. Morph.* **203**, 107–116.

STARMÜHLNER, F. (1956). Beiträge zur Mikroanatomie und Histologie des Darmkanals einiger Opisthobranchier. I. *Sitzungsberichte d. mathem-naturw. Kl., Abt. I* **165**, 8–152.

SUSSWEIN, A. J., SCHWARZ, M. AND FELDMAN, E. (1986). Learned changes of feeding behavior in *Aplysia* in response to edible and inedible foods. *J. Neurosci.* **6**, 1513–1527.

TEYKE, T., WEISS, K. R. AND KUPFERMANN, I. (1990). An identified neuron (CPR) evokes neuronal responses reflecting food arousal in *Aplysia*. *Science* **247**, 85–87.

WEISS, K. R., BREZINA, V., CROPPER, E. C., HOOPER, S. L., MILLER, M. W., PROBST, W. C., VILIM, F. S. AND KUPFERMANN, I. (1992). Peptidergic co-transmission in *Aplysia:* Functional implications for rhythmic behaviors. *Experientia* **48**, 456–463.

WEISS, K. R., CHIEL, H. J., KOCH, U. AND KUPFERMANN, I. (1986). Activity of an identified histaminergic neuron and its possible role in arousal of feeding behavior in semi-intact *Aplysia. J. Neurosci.* **6**, 2403–2415.

WEISS, K. R., KOCH, U. T., KOESTER, J., ROSEN, S. C. AND KUPFERMANN, I. (1982). The role of arousal in modulating the feeding behavior of *Aplysia:* Neural and behavioral studies. In *The Neural Basis of Feeding and Reward* (ed. B. G. Hoebel and D. Novin), pp. 25–57. Brunswick, ME: Haer Institute.

ZIV, I., LUSTIG, C., MARKOVICH, S. AND SUSSWEIN, A. J. (1991). Sequencing of behaviors in *Aplysia fasciata:* Integration of feeding, reproduction and locomotion. *Behav. neural Biol.* **56**, 148–169.